Channel density and efficiency optimization of spectral beam combining systems based on volume Bragg gratings in sequential and multiplexed arrangements

G. B. Ingersoll* and J. R. Leger

Department of Electrical and Computer Engineering, University of Minnesota, 200 Union St. SE, Minneapolis, Minnesota 55455, USA
Corresponding author: gbingersoll@gmail.com

Spectral-beam-combining (SBC) systems utilizing multiple volume Bragg gratings must be carefully analyzed to maximize channel density and efficiency, and thus output radiance. This analysis grows increasingly difficult as the number of channels in the system increases, and heuristic optimization techniques are useful tools for exploring the limits of these systems. We explore three classes of multigrating SBC systems: cascaded, where each grating adds a new channel to the system in sequence; sandwiched, where several individual gratings are placed together and all channels enter the system at the same facet; and multiplexed, where all of the gratings occupy the same holographic optical element (HOE). Loss mechanisms differ among these three basic classes, and our optimization algorithm shows that the highest channel density for a given minimum efficiency and fixed operating bandwidth is achieved for a cascaded grating system. The multiplexed grating system exhibits the lowest channel density under the same constraints but has the distinct advantage of being realized by a single HOE. For a particular application, one must weigh channel density and efficiency versus system complexity when choosing among these basic classes of SBC systems. Additionally, one may need to consider the effects of finite-width input beams. As input beam radius is reduced, angular clipping effects begin to dominate over spectral interference and crosstalk effects, limiting all three classes of SBC systems in a similar manner. © 2015 Optical Society of America

OCIS codes: (090.7330) Volume gratings; (090.6186) Spectral holography; (230.1950) Diffraction gratings.

http://dx.doi.org/10.1364/AO.54.006244

1. INTRODUCTION

Spectral beam combining (SBC) systems are used to generate high laser radiance from several lower-radiance sources. Unlike coherent beam combining systems, the input sources for an SBC system all operate at different wavelengths, so the higher power at the output comes at the expense of a wider output bandwidth. However, SBC systems can be simpler to realize as they are not subject to constraints on the relative phases of the sources [1].

The literature proposes several architectures for SBC systems involving various fundamental optical components. The dispersion from a prism or from surface-relief diffraction gratings is often employed (in reverse) to combine several channels of different wavelengths [2–5]. However, one drawback of these systems is that they tightly couple the positions and wavelengths of the sources through the well-known grating equation.

Coupling between source position and wavelength can be removed by utilizing volume holograms, where an individual volume Bragg grating (VBG) is used for each spectrally distinct source. Systems which only combine two beams often use a single transmission-mode VBG which diffracts one of the beams while the other passes through undiffracted [6]. Those combining more than two beams often utilize several individual reflection-mode VBGs which are organized sequentially such that another input source is added to an intermediate beam at each stage [7,8]. Finally, there are SBC systems—and analogous wavelength division multiplexing systems [9]—that employ a separate transmission-mode VBG for each input channel but multiplex these gratings in a single holographic optical element (HOE). This last system has obvious practical advantages because only a single optical element is required and alignment is simplified.

A goal of many SBC systems is to increase output radiance in a manner that minimizes increases in output bandwidth. Equivalently, the goal is to increase the number of input channels operating within a fixed output bandwidth. Channel density cannot be increased without limit, of course, due primarily

to crosstalk effects among channels. In this work, we compare the relative merits and limitations of sequential grating and multiplexed grating transmission-mode VBG systems. We first explore the differing design constraints and loss mechanisms between these system types. We then introduce an optimization heuristic that reveals regions of the design space which provide the highest channel densities for planewave and finite-beam inputs.

2. VOLUME GRATINGS IN SBC SYSTEMS

We explored three classes of SBC systems based on volume Bragg gratings. The first two utilize gratings in sequential arrangements, whereas the third class of system utilizes a single HOE composed of multiplexed gratings.

We have termed the first type of sequential grating system a cascaded system. A notional schematic of a three-channel cascaded grating system is shown in Fig. 1. In this system, inputs A, B, and C operate at different wavelengths and are combined into output D. At each stage, a separate HOE is used to add the input channel to the intermediate beam. In the ideal case, input A passes through both gratings unchanged, input B is diffracted by the first grating with 100% efficiency and passes through the second grating unchanged, and input C is diffracted by the second grating without loss.

It is notable that while Fig. 1 depicts a transmission-mode system and we only consider transmission-mode systems here, many sequential systems utilize reflection-mode gratings to achieve a nearly flat passband in terms of angular detuning from the Bragg condition (see, e.g., [10]). This improves performance when nonplanewave inputs are used. We explore finite beam inputs further in Section 3.B.

A disadvantage of the cascaded arrangement is the physical size required to allow input beams to enter the system between the HOEs. If we eliminate this space, we arrive at the sandwiched grating arrangement depicted in Fig. 2. Again, in the ideal case, a particular input would be diffracted strongly by one grating and unaffected by the other gratings. The exception is, of course, input A—the "through-beam"—which is ideally not affected by any grating. In contrast to the cascaded arrangement, though, here all inputs pass through all of the
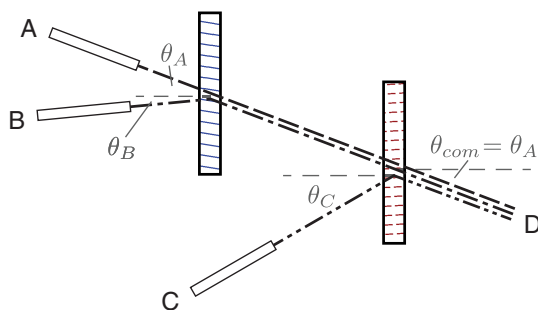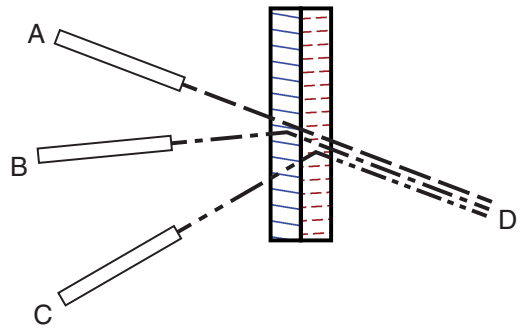

Fig. 2. Three-channel transmission-mode sandwiched grating SBC system utilizing two single-grating HOEs. Inputs A, B, and C operate at different wavelengths and are combined into output D. Ideally, input A is not diffracted by either grating, input B is strongly diffracted by the first grating and not diffracted by the second, and input C is strongly diffracted by the second grating and not diffracted by the first.

HOEs, increasing opportunities for loss due to spurious diffraction in the nonideal case.

Finally, the multiplexed grating system is shown in Fig. 3. Here each of the sinusoidal index of refraction patterns typical of volume phase gratings are present simultaneously in the same HOE.

A. Single VBG System

The simplest case of an SBC system based on volume Bragg gratings is a two-channel system utilizing one grating. This is, in fact, a degenerate case of the three system classes previously introduced. If we assume planewave inputs linearly polarized perpendicular to the plane of incidence, the diffraction efficiency of the single grating as a function of wavelength can be calculated using Kogelnik's well-known coupled-wave method [11]. This appears as shown in Fig. 4 for the two channels' input angles where we assume a material thickness of $d = 0.5$ mm, a common output angle for the system of $\theta_{com} = \theta_A = 0°$, an input angle for input B of $\theta_B = 40°$, and an index modulation for the grating such that 100% diffraction efficiency is achieved for input B.

Conceptually, to achieve 100% efficiency for the single-grating, two-channel system with planewave inputs, one simply
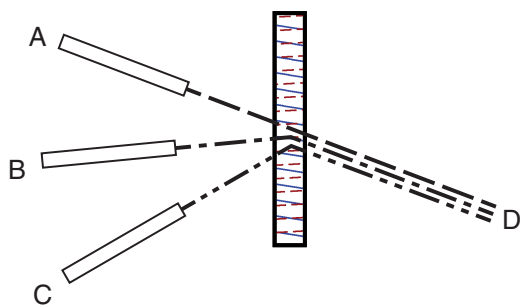

Fig. 1. Three-channel transmission-mode cascaded grating SBC system utilizing two single-grating HOEs. Inputs A, B, and C operate at different wavelengths and enter the system at angles θ_A, θ_B, and θ_C, respectively. These inputs are combined into output D, which leaves the system at angle $\theta_{com} = \theta_A$.

Fig. 3. Ideal three-channel transmission-mode multiplexed grating SBC system utilizing a dual-grating HOE. Inputs A, B, and C operate at different wavelengths and are combined into output D. Ideally, input A is not diffracted by either grating and inputs B and C are each strongly diffracted by one of the multiplexed gratings but not the other.
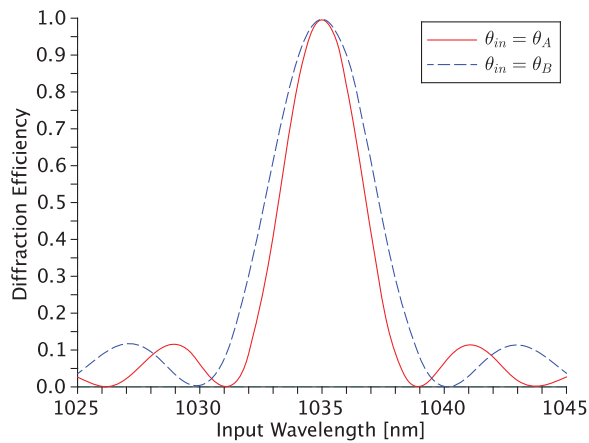
Fig. 4. Diffraction efficiency of a single volume Bragg grating as a function of wavelength for input angles corresponding to the two channels combined by this HOE. The grating parameters are described in the main text. Note how the horizontal scaling of the diffraction efficiency curve varies depending on which input angle is used.

Fig. 5. Diffraction efficiency curves versus wavelength for two gratings, G1 and G2, in a sequential grating SBC system for the input angles corresponding to inputs A and B.

sets the wavelength for input A, λ_A, to one of the zeros of the diffraction efficiency curve when calculated for an input angle of θ_A (e.g., $\lambda_A \approx 1039$ nm). In this manner, the minimum output bandwidth achievable in this two-channel system is dependent on the parameters that define the grating. In general, though, it is well known that increasing the thickness of the grating or utilizing steeper input and output angles—here, making the output angle more negative—will increase the spectral selectivity of the grating, reducing the spacing between the first zeros and minimizing the output bandwidth of this system. The spectral selectivity, $\Delta\lambda$, of this grating can be defined as [12, Eq. 9.88]

$$\Delta\lambda \approx \frac{\Lambda \cot\left(\frac{\theta_B - \theta_{com}}{2}\right)}{d}\lambda_B, \tag{1}$$

where Λ, the grating period itself, also depends on the two angles and the center wavelength of input B, λ_B.

B. Sequential Grating Systems
When one goes beyond a single grating in the system, it becomes increasingly difficult to align diffraction efficiency peaks and zeros. The end result is a system that exhibits unwanted loss due to spurious diffraction. Following inputs A and B through such a system by referring to Fig. 5, the first grating (denoted G1) exhibits 100% diffraction efficiency for an input ($\lambda_B = 1035$ nm, θ_B), and the second grating (denoted G2) exhibits essentially 0% diffraction efficiency for an input (λ_B, θ_{com}). We therefore can expect input B to traverse the system without loss. However, there is no wavelength for which both gratings exhibit 0% diffraction efficiency for input A incident at $\theta_A = \theta_{com}$, so we expect some loss for that channel. ($\lambda_A = 1026$ nm would provide close to ideal performance.)

Again referring to Fig. 5, input C in a cascaded arrangement (see Fig. 1) would only interact with the second grating, so 100% diffraction efficiency could be expected. However, for no loss in a sandwiched arrangement (Fig. 2), there would need
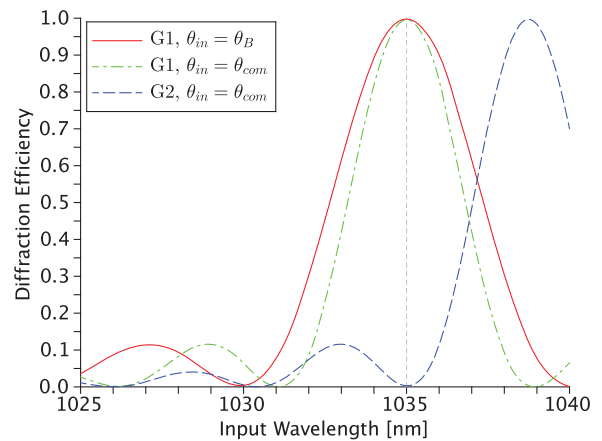
to be an operating point (λ_C, θ_C) where the diffraction efficiency of grating 1 is 0% while the diffraction efficiency of grating 2 is 100%. Inputs B and C necessarily enter the system at different angles (i.e., $\theta_B \neq \theta_C$), so low loss for both channels could be relatively easily achieved at the second grating. However, one can see how the general conditions of low loss, multiple gratings, and narrow, fixed bandwidth are quite difficult to achieve simultaneously.

C. Multiplexed Grating Systems
The loss mechanisms for a multiplexed grating arrangement are more complex still. When more than one grating is present in a single HOE, one can no longer merely attempt to align appropriate peaks and zeros in the various individual diffraction efficiency curves. Rather, the gratings must be treated simultaneously for an input at a particular wavelength and angle, and this forces changes to the set of coupled-wave equations describing the interaction.

Methods appear in the literature for determining and solving the coupled-wave equations describing multiplexed transmission phase gratings. There are analytical methods covering cross-coupling and intergrating interference for dual-grating monochromatic systems [13–15]. In addition, there are methods covering the more general case of polychromatic systems [16].

In a recently published work by the authors [17], an algorithmic approach for calculating diffraction efficiencies in multiplexed grating HOEs was presented. We will use this approach in the studies presented in Section 3. Briefly, this method builds upon the coupled-wave equations of Kogelnik [11] to algorithmically construct a matrix equation describing energy transfer among a set of significant waves within the HOE. For a single grating, it is assumed that only two significant waves are present in the HOE, and the coupled-wave equations of Kogelnik are

$$c_R R' = j\kappa S, \tag{2a}$$

$$c_S S' - j\vartheta S = j\kappa R, \tag{2b}$$

where R and S refer to the complex amplitudes of the "Reference" and "Signal" waves, respectively, and are functions of z, the distance traveled through the HOE. Primes indicate first derivatives in z. κ is the coupling coefficient and is a function of the index modulation, n_1, of the grating and the operating wavelength, and c_R and c_S are the direction cosines of the respective waves. ϑ is the so-called dephasing parameter and is a function of the vector combination of the input wavevector and the grating vector. The value of ϑ is 0 if the input is Bragg-matched with the grating but grows large as the input is detuned from the Bragg condition in angle and/or wavelength. Solving these two equations simultaneously and imposing boundary conditions at the input [i.e., $R(0) = 1$ and $S(0) = 0$] allows one to calculate the energy distribution between the waves at the output [i.e., $R(d)$ and $S(d)$], and thus the diffraction efficiency of the grating for the given input.

For additional gratings in an HOE to be properly handled, the set of differential equations in Eq. (2) must be expanded and solved simultaneously. In particular, the authors' method involves combining the input wavevector with each grating vector—and indeed various sum and difference combinations of the grating vectors—to build a full set of M waves within the material and thus a full set of coupled differential equations represented by an $M \times M$ matrix. Determining the energy distribution among all of the significant waves at the output and their associated diffraction efficiency values involves eigenvector decomposition of this matrix and again imposing appropriate boundary conditions.

Fortunately many combinations of the input wavevector and the grating vectors result in large associated values of ϑ, and the corresponding waves may be safely disregarded. Nonetheless, for systems of many gratings, M can grow quite large. The consequence of these additional coupled waves for a multiplexed grating SBC system is increased spurious diffraction (cross-coupling or intergrating interference), resulting in decreased efficiency relative to a similar sequential grating system.

In a sandwiched or cascaded grating arrangement, the system of two gratings explored in Fig. 5 was expected to provide near 100% system efficiency for its three inputs. If we collapse those two gratings into a single HOE to create a multiplexed grating arrangement, though, the resulting calculated efficiency values are significantly different as shown in Fig. 6. Here, both inputs B and C are subject to efficiency losses greater than 10% at their respective wavelengths due to spurious waves and grating cross-coupling occurring within the single HOE.

Some insight can be gained by investigating the diffraction efficiency for input B as a function of depth, z, in the grating as shown in Fig. 7. This essentially depicts the transfer of energy between the given input wave and desired output wave, as these waves travel through the HOE from $z = 0$ to $z = d$, where d is the thickness of the material. One curve in the figure represents this energy transfer for an HOE with only Grating 1 present, and we can see that the curve reaches 100% energy transfer at $z = d$ as desired. The other curve, though, represents this energy transfer with Grating 2 present in the HOE as well, and we can see that not only does the energy transfer peak occur for $z \neq d$, but, more importantly, the curve
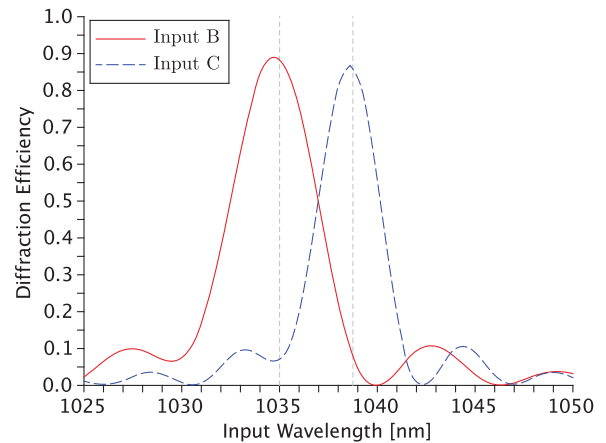

Fig. 6. Diffraction efficiencies at the system output for inputs B and C of a two-grating multiplexed SBC system formed by trivially collapsing the two gratings of a sandwiched grating system into a single HOE.

never reaches 100% energy transfer. In general, some of the energy that is not transferred into the output wave of interest remains in the input wave and some is diffracted into a spurious wave.

Clearly it is nontrivial to design an SBC system, especially as the number of channels increases. Given physical constraints (overall size, input angles, etc.) on a sequential grating system, it is not practical in general to achieve perfect alignment of all pertinent combinations of diffraction efficiency peaks and zeros for all gratings. Multiplexed grating systems, despite the advantages that come with having a single HOE, further suffer from intergrating interference effects within that single HOE.

For some applications, it has been correctly suggested that cross-coupling and intergrating interference effects can be essentially eliminated through wide separation of channel
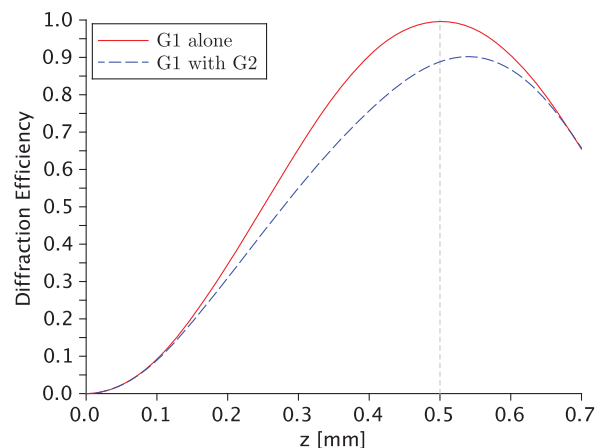

Fig. 7. Diffraction efficiency of Grating 1 as a function of HOE depth, z, for input B satisfying the Bragg condition. The solid red curve shows the efficiency with Grating 1 alone (i.e., Grating 2 is not present in the HOE). The dashed blue curve shows the effect of adding Grating 2 to the HOE. The vertical dashed line indicates $z = d$, where d is the thickness of the HOE.

wavelengths [18,19]. This, however, is counter to our goal of maximizing channel density in an SBC system given a fixed operating bandwidth.

In the next section, we introduce an optimization method that aims to find design parameters for SBC systems which provide the highest overall efficiency for a fixed system bandwidth given the number of channels in the system. Using this method, we compare the relative channel density limits of the different classes of SBC systems. We further explore the effects of nonplanewave inputs on system performance.

3. SBC SYSTEM OPTIMIZATION

Optimizing a multigrating SBC system is a nonlinear problem of many dimensions. In order to explore the solution spaces for multiplexed and sequential grating systems, we employ a computationally efficient metaheuristic algorithm. We apply practical constraints to each system variable and then use particle swarm optimization (PSO) [20] to determine a set of parameters that results in the SBC system with the highest overall efficiency.

We define three system-wide variables that are held constant for a given optimization run: the number of channels, N; the material thickness, d; and the common output angle, θ_{com}. Further, the optimizer adjusts three grating variables for each channel: center wavelength (λ_{center}), input angle (θ_{in}), and index modulation n_1. To compare the effects of different values of the system-wide variables, we optimized cascaded, sandwiched, and multiplexed grating SBC systems in the four groups summarized in Table 1. For all four groups, we keep the operating bandwidth of the system fixed at 1030–1040 nm.

We chose the two values for d in Table 1 to be sufficiently different to allow us to show trends in the effect of material thickness on channel density and system efficiency. Further, we chose these thickness values to be relatively small in order to limit the maximum value of N that we needed to consider in the optimization runs. As discussed in Section 3.A, as the material thickness under consideration increases, the number of channels supported in an efficient system also increases, resulting in much longer execution times for the optimizer without providing additional insight into the general problem. A similar argument applies to the selection of values for θ_{com}.

Within each of the four groups, we explored several values of N. In each case, the optimizer adjusts $3N$ parameters (i.e., three grating variables times N channels) which are allowed to vary over the ranges summarized in Table 2. Early experiments with this method revealed that the optimizer tended to space channels equally within the given fixed operating bandwidth. To improve the efficiency of the algorithm, we then

Table 1. System-Wide Variable Constraints Placed on the Optimization Algorithm for Each of the Four Simulation Groups

	d [μm]	θ_{com}
Group 1	500	0°
Group 2	500	−30°
Group 3	1000	0°
Group 4	1000	−30°

Table 2. Constraints Placed on the Optimization Algorithm for Each of the Gratings' Three Independent Variables

λ_{center}	±1 nm variation around evenly spaced channels within fixed bandwidth
θ_{in}	35°–50°
n_1	Kogelnik result $\pm 5 \times 10^{-5}$

modified it to assume small adjustments to channel wavelengths around this equal spacing. This eliminates large volumes of the $3N$-dimensional search space where results are known to be quite poor. Likewise, the index modulation for each grating is allowed to vary over a narrow range around the value that would give the grating 100% efficiency in Kogelnik's calculation for a single lossless transmission grating.

The particle swarm is initialized with 200 particles uniformly distributed within the search space with zero velocity. In each iteration, each particle's energy is calculated using a metric based on the represented SBC system's total diffraction efficiency (i.e., the sum of the diffraction efficiencies at each channel's input angle and center wavelength). The best energy for each particle and for the swarm of particles as a whole is tracked, and each particle's new velocity vector, $\boldsymbol{v}_{n+1}$, and new position vector, $\boldsymbol{p}_{n+1}$, are calculated as follows:

$$\boldsymbol{v}_{n+1} = \omega \boldsymbol{v}_n + \phi_p r_p \Delta_{p,best} + \phi_g r_g \Delta_{g,best}, \tag{3}$$

$$\boldsymbol{p}_{n+1} = \boldsymbol{p}_n + \boldsymbol{v}_{n+1} \times (1\text{ iteration}), \tag{4}$$

where ω, ϕ_p, and ϕ_g are tuning constants for the simulation; $\Delta_{p,best}$ and $\Delta_{g,best}$ are the Euclidean distances between the given particle and the particle's and swarm's (respectively) best-known positions; and r_p and r_g are uniformly distributed random numbers between 0 and 1 that are updated for each calculation. If an element of a particle's new position vector exceeds the defined limits of the search space, that element is set to the nearest boundary and the corresponding element of the particle's velocity vector is set to 0.

Given finite execution time, PSO does not guarantee finding the global optimum. However, by adjusting the simulation variables ω, ϕ_p, and ϕ_g, the convergence of the simulation can be adjusted to avoid converging too quickly to a local minimum and also to avoid converging too slowly in general. Examining Eq. (3), ω is analogous to the particle's inertia, and ϕ_p and ϕ_g are analogous to gravity pulling the particle toward the particle's and swarm's best-known positions. The values of these variables were determined through experimentation and are initialized in the optimizer to 0.80, 0.30, and 0.05, respectively. The optimizer runs for 200 iterations, and after 170 iterations these values are changed to 0.55, 0.25, and 0.15, respectively, to accelerate convergence to the swarm's best-known position and increase the number of particles in the vicinity of that position to fine-tune the result. To reinforce the validity of these tuning parameters, we executed the optimizer multiple times under the same constraints and compared the results, expecting the optimizer to return a system with comparable efficiency each time. The consistency of the results of multiple runs shown in Section 3.A indicates that these tuning parameter

values slow convergence of the swarm sufficiently to avoid local extrema, while still allowing consistent convergence within the 200 iteration limit imposed to maintain a practical maximum execution time on the order of hours.

The next section explores optimization results for planewave inputs; then the following section explores optimization results when inputs of finite transverse extent are taken into account.

A. Results for Planewave Inputs

In the following subsections, we present system efficiency results for optimized multiplexed and sequential grating SBC systems operating between 1030 and 1040 nm for increasing numbers of channels. Note that in these simulations, we do not include the through-channel (e.g., channel A in Fig. 1). Rather, we only include diffracted channels for which there is an associated grating. The parameters of the through-channel do impact system performance, but neglecting the through-channel in the optimization algorithm reduces the dimensionality of the system, which reduces optimization time. To add the through-channel to a system, one would optimize over a band slightly narrower than the desired operating band and then add the through-channel on either end of the band following optimization either manually or via a separate algorithm.

1. Multiplexed Grating Systems

We executed the optimizer for multiplexed grating SBC systems for each of the four system parameter groups (Table 1) for up to 14 channels and an operating band covering 1030–1040 nm. In each case, we repeated the optimization five times to check consistency, and results are plotted in terms of system efficiency in Fig. 8. System efficiency for each group decreases from near 100% as the number of channels increases and intergrating interference effects begin to compromise performance. Note that as efficiency falls off for a given group, optimization consistency also decreases. Intergrating interference in these arrangements strongly limits the achievable system efficiency, resulting in many solutions with relatively
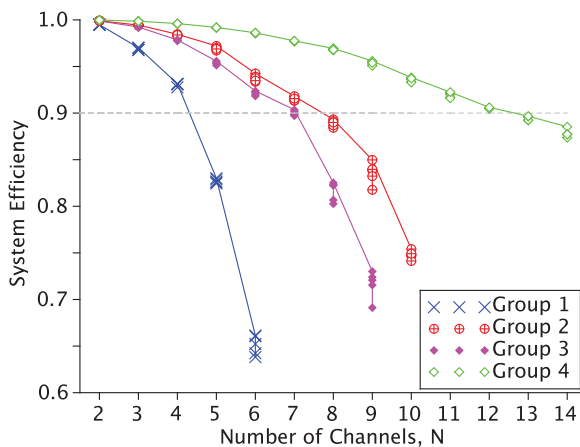
poor performance. Given the optimizer's finite execution time, the best of the poor solutions is not always discovered.

All four groups perform similarly—and rather well—until four channels are included in the system. At this point, the intergrating interference in Group 1 (i.e., the thinner material and shallower output angle) begins to compromise system performance. The remaining three groups continue to perform well until eight channels are employed when the curves for Groups 2 and 3 drop below the horizontal line, indicating 90% system efficiency. It is clear from Fig. 8 that Group 2 performs slightly better than Group 3 as the number of channels in the system is increased. This suggests that given the basic constraints we have placed on the system (i.e., operating bandwidth, operating angles, thicknesses), a steeper output angle has more of an effect on wavelength selectivity [see Eq. (1)] of a given grating than material thickness although this is not necessarily the case in general. Finally, using both a thick material and a steep output angle (i.e., Group 4) exhibits the best performance of all four groups, allowing greater than 50% more channels than the next best group if we enforce a system efficiency limit of 90%.

2. Sequential Grating Systems

Like with the multiplexed grating systems, we also executed the optimizer for cascaded and sandwiched grating SBC systems for each of the four groups, and for up to 20 channels and an operating band again covering 1030–1040 nm. The results for the cascaded systems are plotted in terms of system efficiency in Fig. 9. Again, system efficiency for each group decreases as the number of channels in the system is increased and cross-coupling effects become more prominent. In a similar fashion to the multiplexed grating system, Group 1 is the worst performer, Group 4 the best, and Group 2 slightly outperforms Group 3. This reinforces the notion that steep output angles and thick materials improve channel density, and for the ranges of parameters considered here, a steep output angle improves
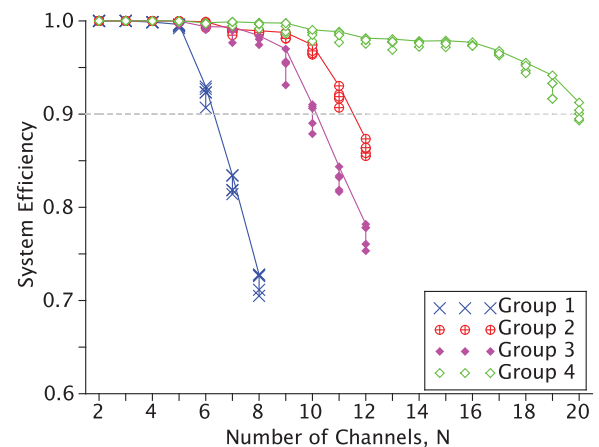

Fig. 8. Optimized multiplexed grating system efficiency for each of the four system parameter groups as a function of the number of channels in the system, N. Operating bandwidth is fixed at 1030–1040 nm. The dashed horizontal line indicates an arbitrary system efficiency goal of 90%. Stacked symbols indicate the results of repeated optimizer runs for a given set of inputs.

Fig. 9. Optimized cascaded grating system efficiency for each of the four system parameter groups as a function of the number of channels in the system, N. Operating bandwidth is fixed at 1030–1040 nm. The dashed horizontal line indicates an arbitrary system efficiency goal of 90%. Stacked symbols indicate the results of repeated optimizer runs for a given set of inputs.

channel density somewhat more than a thicker holographic material.

The key comparison, though, is the performance of multiplexed grating systems and sequential grating systems within the same group. The differing nature of the interference in a sequential system discussed in Section 2 allows for many more channels than in a multiplexed grating system, regardless of group, before system efficiency is compromised. Using 90% system efficiency as a basic metric and referencing Figs. 8 and 9, for each of the four groups, the cascaded grating arrangement supports roughly 50% more channels than the multiplexed arrangement in the same group.

Results for sandwiched grating systems are not plotted here for brevity. As one might expect, though, these systems outperform multiplexed grating systems group by group. However, they do not perform as well as cascaded grating systems because every input must interact with every grating in the sandwiched grating arrangement, which increases loss. Efficiency of 90% was achieved for the sandwiched grating arrangement for 6, 10, 9, and 17 channels for Groups 1–4, respectively.

These results do not suggest, though, that for a practical case a sequential grating system should always be preferred over a multiplexed grating system. First, in the optimization calculations, the fixed material thickness is used on a per-grating basis in order to keep the spectral widths of the channels relatively constant. So if an N-channel multiplexed grating system has a thickness d—with all gratings sharing the same slab of material—an N-channel sandwiched grating system would have a thickness of Nd with each grating occupying a separate slab of material and a cascaded grating system would be larger still because of the spacing between the individual HOEs. If instead we assume that each grating in a sequential system had a thickness of d/N, the spectral widths of the resulting gratings' efficiency curves would be very wide and intergrating interference would be severe. The multiplexed system would outperform the sequential system in every case.

In addition to the difference in the overall system thickness, other practical considerations need to be made when choosing between a sequential arrangement and a multiplexed one. These include ease and repeatability of assembly, alignment, and thermal management. Depending on these other factors, a multiplexed grating architecture may be preferred in some cases despite lower efficiency for a given number of channels. However, these considerations must also be weighed against limitations to the number of gratings that can be successfully multiplexed given the dynamic range of the holographic medium and difficulties arising from multiple exposures (e.g., partial erasure) [21].

B. Results for Finite Beam Inputs

An important factor that is not considered in the results of the previous section is the angular acceptance of the constituent volume Bragg gratings in these types of SBC systems (i.e., how diffraction efficiency decreases for inputs mismatched in angle from the Bragg condition). Until now, only planewave inputs have been considered in the system optimization algorithm, and as we have shown, parameter groups involving steeper output angles and thicker materials exhibit higher efficiency at higher channel counts. It is clear that favoring these

parameters improves channel density because the spectral width of a grating's diffraction efficiency curve narrows as steeper angles and thicker materials are used. This reduction in spectral width for a given grating correlates with a reduction in the effects of intergrating interference for a given number of channels and a fixed operating spectrum. However, similar narrowing is evident in the *angular* width of the grating's diffraction efficiency curve. If we assume Gaussian inputs of various radii instead of planewave inputs, and we consider the angular planewave spectra of these inputs when calculating the diffraction efficiency for each channel (see, e.g., [22]), there must be a compromise between increasing angles and/or thickness to narrow spectral width (i.e., to increase channel density) and decreasing angles and/or thickness to improve angular acceptance (i.e., to reduce per-channel loss due to nondiffracted power).

The relative sizes of the angular acceptance curve of a typical Group 1 grating and the angular planewave spectra for various Gaussian beam widths (assuming a wavelength of 1035 nm) are depicted in Fig. 10. Clearly, even for a beam radius of 1 mm, the width of the beam's angular planewave spectrum is significant relative to the width of the central lobe of the grating's diffraction efficiency curve. This will result in a decrease in per-channel efficiency independent of intergrating interference effects.

The following sections present optimization results for SBC systems accounting for these finite input widths. The optimization algorithm was modified to use the beam radius as an additional system-wide variable. Diffraction efficiencies at 15 angles between the $1/e^2$ points of the Gaussian angular planewave power spectrum are weighted, calculated, and combined to give an aggregate diffraction efficiency for that channel given the beam radius. (Beam shape and beam quality are not considered here.)

1. Output Angle Optimization

We begin by keeping the thickness of the holographic material fixed at 0.5 mm and allowing the optimizer to vary the channels' common output angles between 0° and –30°. That is, in addition to selecting center wavelengths, modulation levels,
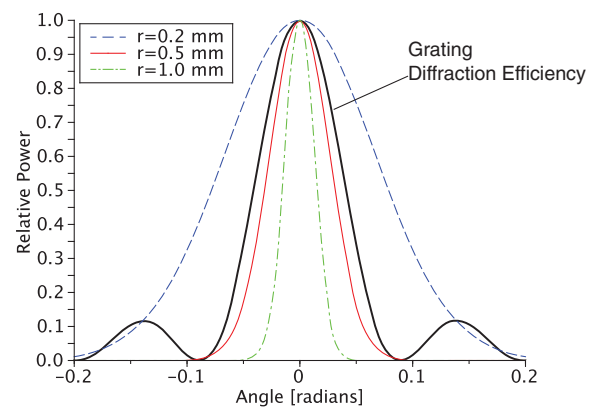

Fig. 10. Relative angular widths for Gaussian inputs at 1035 nm with various radii compared with the diffraction efficiency as a function of input angle (for a fixed wavelength) of a typical Group 1 grating centered at 1035 nm.
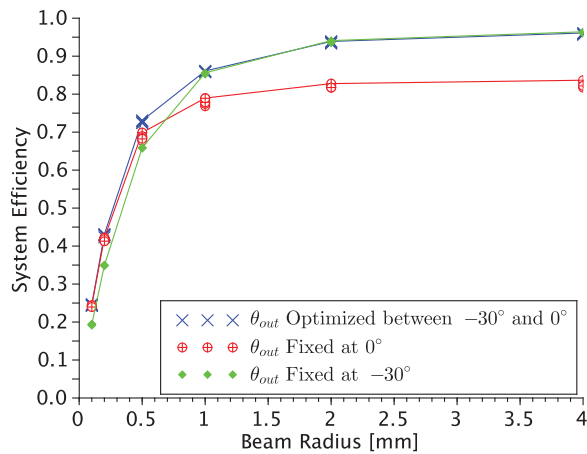
Fig. 11. Efficiency of a five-channel multiplexed grating system as a function of input beam radius. The material thickness is kept constant at 0.5 mm. The three curves indicate the efficiency results with the system output angle fixed at 0° (Group 1), fixed at –30° (Group 2), and optimized between those two angles. Stacked symbols indicate the results of repeated optimizer runs.

Fig. 12. Optimized output angle for a five-channel multiplexed grating system as a function of input beam radius. The material thickness is kept constant at 0.5 mm. Stacked symbols indicate the results of repeated optimizer runs, and the solid line indicates the angles associated with the highest achieved system efficiency (see Fig. 11) for a given input beam radius.

and input angles for each channel, the optimizer is also choosing a common output angle for the system between the angles previously defined for Groups 1 and 2.

The system efficiency results as a function of beam radius for this exercise are shown in Fig. 11 for a five-channel multiplexed grating system. Also depicted for comparison are the optimization results if the system output angle is kept fixed at 0° (Group 1) and –30° (Group 2).

For a large beam radius, the angle-optimized system performs as well as the Group 2 system. This is because, for large beam radius, the system is not constrained by angular clipping and the optimizer simply selects the steepest allowed output angle (–30° in this case) to minimize intergrating interference. However, as the beam radius decreases, the efficiency of the Group 2 system falls off more quickly than the other systems due to clipping of the inputs' angular planewave spectra.

At a radius of 0.5 mm, the angle-optimized system exhibits the highest efficiency because it uses an output angle that is a compromise between angular clipping and intergrating interference. For this input radius, the steeper –30° output angle gives rise to clipping of the angular spectra of the inputs while the shallower 0° output angle results in a system that is limited by intergrating interference.

For radii less than 0.5 mm, the effect of angular clipping supersedes the effect of intergrating interference and the performance of the angle-optimized system converges with the Group 1 system. That is, the optimizer selects the shallowest available angle to minimize per-channel loss due to angular clipping despite the intergrating interference that is also present.

The output angles selected by the optimizer are plotted versus input beam radius in Fig. 12. The trend of the optimizer selecting a shallower common output angle for small beam radii is clear. Note, though, the relative inconsistency of the selected output angle for small radii shown in Fig. 12 despite the consistency in the system efficiency from the same optimization
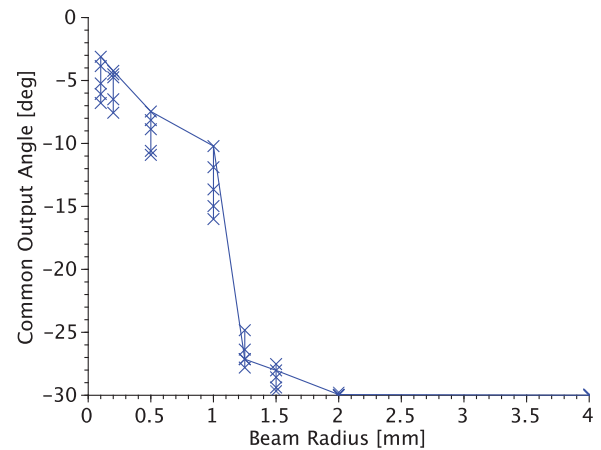
runs shown in Fig. 11. This suggests that as the best attainable system efficiency—the parameter that the algorithm is optimizing—decreases, there are many combinations of system parameters that can achieve that efficiency as angular clipping is traded against intergrating interference.

Similar data for output angle optimization in both a cascaded and sandwiched grating system was generated but is not included here. The trends are similar to the multiplexed grating system. For large input beam radii, the optimizer tends toward the steepest output angle available to minimize cross-coupling among the gratings. As the input beam radius decreases, the optimizer decreases the common output angle of the system to reduce clipping of the input beams resulting from the narrow angular response of the grating despite increasing cross-coupling.

Again, of course, the overall efficiency of these sequential arrangements decreases dramatically as the input beam radius drops below approximately 1 mm just like the multiplexed grating arrangement. Given the constraints of a particular group and a fixed operating bandwidth, there is a beam radius below which angular clipping effects dominate, resulting in poor performance regardless of whether the SBC system uses multiplexed or sequential gratings.

2. Output Angle and Thickness Limitations

In the previous section, we used our PSO algorithm to select an optimum output angle for an SBC system in addition to optimizing the parameters for each diffracted channel. This was performed for a range of beam radii but for a fixed thickness. In this section, we show optimization results for multiplexed grating SBC systems over variation in hologram thickness as well. Again, for each case the optimization algorithm arrives at the best common output angle for the system given other parameters, although the final output angles are not shown here.

Figure 13 shows regions of the holographic element thickness (d) versus beam radius (r) space for which $\geq 90\%$ system
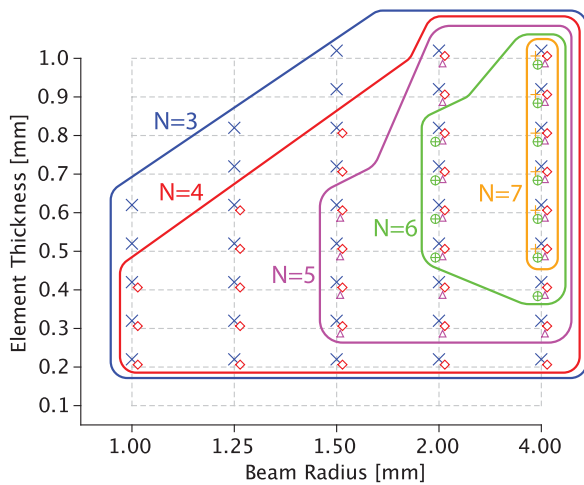
Fig. 13. Regions of beam radius (*r*) and holographic element thickness (*d*) where 90% system efficiency can be achieved in a multiplexed grating architecture for various numbers of channels *N*. The PSO optimizer was executed for combinations of thickness and radius at the intersections of the dashed lines, and the mark representing a particular number of channels is included at an intersection if the optimized system efficiency exceeded 90%.

efficiency can be achieved in a multiplexed grating system for a given number of channels. In the upper right of the plot (i.e., for inputs approaching planewaves and for thicker materials), the highest numbers of channels are supported. With (near) planewave inputs, the systems are not limited by angular clipping, so the optimizer is free to choose the steepest available output angle (−30°) and the results approach the Group 4 results shown in Fig. 8. That is, for $r = \infty$—or, in fact, $r \geq$ 4.00 mm for the systems described—and $d = 1.00$ mm, a multiplexed grating system can support $N \leq 12$ with at least 90% efficiency, or $N_{max} = 12$. (Note that the plot only shows up to $N = 7$ for clarity.)

Continuing clockwise to the lower-right region of Fig. 13, we can see the effects of intergrating interference on overall system efficiency. As the thickness of the material decreases to 0.5 mm, the optimizer again favors a steeper common output angle, and the results match the Group 2 results in Fig. 8 for planewave inputs ($N_{max} = 7$). The optimizer is not allowed to increase the common output angle beyond −30°, so as the hologram thickness decreases below 0.5 mm, N_{max} decreases due to intergrating interference.

Moving to the lower-left region of Fig. 13, there is not a significant difference in N_{max} as the beam radius decreases. In this region, the material is relatively thin and the optimizer can additionally reduce the common output angle, both of which tend to avoid loss due to angular clipping which is typically present for lower values of *r*. However, a thin material and a shallow output angle together lead to significant intergrating interference (cf. Group 1 in Fig. 8), so the number of supported channels, N_{max}, remains small.

Finally, inspecting the upper-left region of Fig. 13, we note that the multiplexed grating system cannot support even a small number of diffracted channels when utilizing thicker materials

and smaller beam radii. $N_{max} \to 0$ simply due to angular clipping.

Similar data to Fig. 13 can be shown for sequential grating systems but is not included here for brevity. The numbers of supported channels under a 90% efficiency constraint follow Fig. 9 for cascaded grating systems as $r \to \infty$. Also, N_{max} falls off quite similarly to the trends shown in Fig. 13 as $r \to 0$ because, again, power loss due to angular clipping affects both sequential and multiplexed grating SBC systems in an essentially equivalent manner.

4. CONCLUSION

SBCs utilizing multiple volume Bragg gratings must be carefully analyzed to maximize performance. This analysis grows increasingly difficult as the number of channels—and therefore the number of variables—increases, and heuristic optimization techniques are useful tools for exploring the limits of these systems.

Of the three system classes discussed, the highest channel densities were achieved by cascaded grating systems because each input beam in such a system only interacts with subsequent gratings in the cascade. However, this also leads to cascaded grating systems being physically larger than the other two classes due to the required spaces between the single-grating HOEs.

Sandwiched grating systems exhibited the next best channel densities, only slightly lower than cascaded grating systems. This decrease is due to each input beam interacting with all of the individual gratings in the system but comes with the advantage of a more compact arrangement.

The multiplexed grating system exhibited the poorest performance of the three system classes. It is also the most difficult to analyze, being subject to intergrating interference effects within its single HOE. Requiring only one HOE, though, is a distinct advantage to this type of system.

Finally, when nonplanewave inputs are used with any of these grating arrangements, overall system efficiency drops quickly as beam radii decrease. This is due to limited angular acceptance in these volume Bragg gratings which affects all three arrangements roughly equally. However, when used in high-power SBC applications, these volume gratings would most likely be designed for use with expanded beams to account for thermal limitations, and less attention would need to be paid to beam radius considerations.

REFERENCES

1. T. Y. Fan, "Laser beam combining for high-power, high-radiance sources," IEEE J. Sel. Top. Quantum Electron. **11**, 567–577 (2005).
2. E. J. Bochove, "Theory of spectral beam combining of fiber lasers," IEEE J. Quantum Electron. **38**, 432–445 (2002).
3. S. Klingebiel, F. Roser, B. Ortac, J. Limpert, and A. Tunnermann, "Spectral beam combining of Yb-doped fiber lasers with high efficiency," J. Opt. Soc. Am. B **24**, 1716–1720 (2007).

4. T. H. Loftus, A. M. Thomas, P. R. Hoffman, M. Norsen, R. Royse, A. Liu, and E. C. Honea, "Spectrally beam-combined fiber lasers for high-average-power applications," IEEE J. Sel. Top. Quantum Electron. **13**, 487–497 (2007).

5. P. Madasamy, D. R. Jander, C. D. Brooks, T. H. Loftus, A. M. Thomas, P. Jones, and E. C. Honea, "Dual-grating spectral beam combination of high-power fiber lasers," IEEE J. Sel. Top. Quantum Electron. **15**, 337–343 (2009).

6. I. V. Ciapurin, L. B. Glebov, L. N. Glebova, V. I. Smirnov, and E. V. Rotari, "Incoherent combining of 100-W Yb-fiber laser beams by PTR Bragg grating," Proc. SPIE **4974**, 209–219 (2003).

7. B. Chann, A. K. Goyal, T. Y. Fan, A. Sanchez-Rubio, B. L. Volodin, and V. S. Ban, "Efficient, high-brightness wavelength-beam-combined commercial off-the-shelf diode stacks achieved by use of a wavelength-chirped volume Bragg grating," Opt. Lett. **31**, 1253–1255 (2006).

8. A. Sevian, O. Andrusyak, I. V. Ciapurin, V. I. Smirnov, G. B. Venus, and L. B. Glebov, "Efficient power scaling of laser radiation by spectral beam combining," Opt. Lett. **33**, 384–386 (2008).

9. S. Datta and S. R. Forrest, "Low through channel loss wavelength multiplexer using multiple transmission volume Bragg gratings," J. Opt. Soc. Am. A **22**, 1624–1629 (2005).

10. D. R. Drachenberg, O. Andrusyak, G. B. Venus, V. I. Smirnov, J. Lumeau, and L. B. Glebov, "Ultimate efficiency of spectral beam combining by volume Bragg gratings," Appl. Opt. **52**, 7233–7242 (2013).

11. H. Kogelnik, "Coupled wave theory for thick hologram gratings," Bell Syst. Tech. J. **48**, 2909–2947 (1969).

12. R. J. Collier, C. B. Burckhardt, and L. H. Lin, *Optical Holography* (Academic, 1971).

13. R. Alferness, "Analysis of optical propagation in thick holographic gratings," Appl. Phys. **7**, 29–33 (1975).

14. R. Alferness and S. K. Case, "Coupling in doubly exposed, thick holographic gratings," J. Opt. Soc. Am. **65**, 730–739 (1975).

15. S. K. Case, "Coupled-wave theory for multiply exposed thick holographic gratings," J. Opt. Soc. Am. **65**, 724–729 (1975).

16. V. Minier and J. M. Xu, "Coupled-mode analysis of superimposed phase grating guided-wave structures and intergrating coupling effects," Opt. Eng. **32**, 2054–2063 (1993).

17. G. B. Ingersoll and J. R. Leger, "Spectral interference in multiplexed volume Bragg gratings: theoretical calculations and experimental verification," Appl. Opt. **53**, 5477–5485 (2014).

18. X. Fu, M. Fay, and T. M. Xu, "18 supergrating wavelength-division de-multiplexer in a silica planar waveguide," Opt. Lett. **22**, 1627–1629 (1997).

19. A. Othonos, J. Bismuth, M. Sweeny, A. Kevorkian, and J. M. Xu, "Superimposed grating wavelength division multiplexing in Ge-doped SiO_2/Si planar waveguides," Opt. Eng. **37**, 717–720 (1998).

20. J. Kennedy and R. Eberhart, "Particle swarm optimization," Proc. IEEE **4**, 1942–1948 (1995).

21. D. Brady and D. Psaltis, "Control of volume holograms," J. Opt. Soc. Am. A **9**, 1167–1182 (1992).

22. B. Benlarbi, P. S. J. Russell, and L. Solymar, "Bragg diffraction of finite beams by thick gratings: two rival theories," Appl. Phys. B **B28**, 63–72 (1982).